Structural Analysis of Lipoprotein E Particles[†]

Lumelle A. Schneeweis,[‡] Vishwanath Koppaka,[‡,§] Sissel Lund-Katz,[∥] Michael C. Phillips,[∥] and Paul H. Axelsen*[,‡]

University of Pennsylvania, Philadelphia, Pennsylvania 19104, and Children's Hospital of Philadelphia, Philadelphia, Pennsylvania 19104

Received May 11, 2005; Revised Manuscript Received July 21, 2005

ABSTRACT: Apolipoprotein E (apoE) is a key regulator of cholesterol homeostasis. Human apoE has three common isoforms, each with different risk implications for cardiovascular and neurodegenerative disease. Neither the structure of lipoprotein E particles nor the structural consequences of the isoform differences are known. In this investigation, synthetic lipoprotein particles were prepared by complexing phospholipids with full-length apoE isoforms, or with truncated N-terminal and C-terminal domains of apoE. These particles were examined with calorimetry, electron microscopy, circular dichroism spectroscopy, and internal reflection infrared spectroscopy. Results indicate that particles made with the three full-length apoE isoforms are discoidal in shape, and structurally indistinguishable. Thus, differences in their pathological consequences are not due to gross differences in particle structure. Although apoE is predominantly helical, and the axes of the helices are parallel to the flat surfaces of the particles, the orientational order of lipid acyl chains is low and inconsistent with the belt model of lipoprotein A-I structure. Instead, the data suggest that there are at least two different types of apoE−lipid interactions within lipoprotein E particles. One type occurs between apoE helices and the edge of the lipid bilayer as in the belt model, while a second type involves apoE helices that situate in the plane of the membrane and disturb acyl chain order. These interactions allow LpE particles to form with different protein/lipid ratios, and they account for the structure of LpE particles made with only the truncated domains.

Apolipoprotein E (apoE)[1] is a 299-amino acid protein that is involved in lipid transport and cholesterol homeostasis. In plasma, apoE is found with other proteins in lipoprotein particles as diverse as chylomicrons and high-density lipoproteins (HDLs), and it is involved in delivering cholesterol to cells expressing the apoB,E LDL receptor as well as other related receptors (*1*). In the brain and cerebrospinal fluid (CSF), apoE is the most abundant apolipoprotein, and it is found in particles that resemble HDL in density and size (*2*). Binding appears to result in delivery of cholesterol to those cells (*3*), a process that is enhanced at sites of nerve damage (*4*).

ApoE exists as three common isoforms in the human population. ApoE3 is the most common (77% of the alleles) and is therefore considered to be the wild type. ApoE2 has an R158C substitution, while apoE4 has a C112R substitution: both are associated with forms of hyperlipidemia (*1*). Persons with one copy of the apoE4 gene also have a 3-fold increased incidence of Alzheimer's disease (AD), while persons with two copies of the gene have an 8-fold increased incidence. The apoE2 gene, however, reduces the incidence of AD by 60% for one apoE2 allele (*5*). Both sites of substitution are in the 22 kDa, N-terminal, domain (*6*). This domain is connected via a protease sensitive hinge region to a 10 kDa C-terminal domain which mediates oligomerization and exhibits a higher affinity for lipids (*7, 8*). An X-ray crystal structure is available for the N-terminal domain of apoE in the absence of lipids (*9*−*12*), and progress is being made toward determining a structure for the lipid-free C-terminal domain by nuclear magnetic resonance (NMR) (*13, 14*).

Prior investigations of apoE structure in lipoprotein complexes have used spectroscopic approaches such as fluorescence resonance energy transfer to measure lipid-induced N-terminal domain conformational changes (*15*), the proximity of apoE α-helices to lipid acyl chain positions (*16*), the α-helix proximity in discoidal lipoprotein particles (*17*), and lipid-induced tertiary domain reorientation (*18, 19*). NMR chemical shift changes in LpE have been used to

[†] This work was supported by NIH Grants HL68186 and AG20238 (P.H.A.) and HL56083 (S.L.-K.).

* To whom correspondence should be addressed. Telephone: (215) 898-8416. Fax: (215) 573-9135. E-mail: axe@pharm.med.upenn.edu.

[‡] University of Pennsylvania.

[§] Current address: BioMarin Pharmaceutical Inc., 46 Galli Dr., Novato, CA 94949.

[∥] Children's Hospital of Philadelphia.

[1] Abbreviations: apoE, apolipoprotein E; LpE, lipoprotein E; PATIR-FTIR, polarized attenuated total internal reflection Fourier tranform infrared spectroscopy; LpA-I, lipoprotein A-I; HDL, high-density lipoprotein; apoB,E LDL receptor, apolipoprotein B,E low-density lipoprotein receptor; DSC, differential scanning calorimetry; DLS, dynamic light scattering; EM, electron microscopy; CD, circular dichroism spectroscopy; DMPC, dimyristoylphosphatidylcholine (di-14:0 PC); DMPS, dimyristoylphosphatidylserine (di-14:0 PS); DPPC, dipalmitoylphosphatidylcholine (di-16:0 PC); DPPS, dipalmitoylphosphatidylserine (di-16:0 PS); POPC, palmitoyloleoylphosphatidylcholine (16:0,18:1 PC); POPS, palmitoyloleoylphosphatidylserine (16:0,18:1 PS); LpE-FL, lipoprotein particles made from any of the full-length isoforms of apoE; LpE2-FL, lipoprotein particles made from full-length apoE2; LpE3-FL, lipoprotein particles made from full-length apoE3; LpE4-FL, lipoprotein particles made from full-length apoE4; LpE-TD, lipoprotein particles made from either of the truncated domains of apoE; $LpE\text{-}TD_{10}$, lipoprotein particles made from the 10 kDa C-terminal domain of apoE; $LpE3\text{-}TD_{22}$, lipoprotein particles made from the 22 kDa N-terminal domain of apoE3; LpA-I-FL, lipoprotein particles made from full-length apoA-I.

10.1021/bi050872j CCC: $30.25
Published on Web 08/23/2005

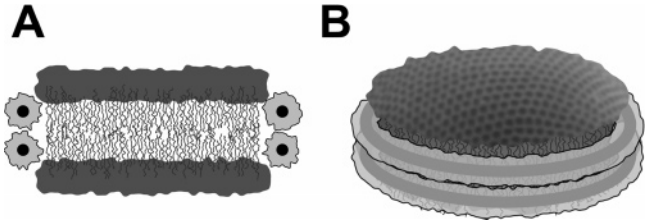

FIGURE 1: Schematic illustration of the belt model for LpA-I structure, based on the all-atom model of Klon et al. (*51*), and drawn to scale. (A) Cross sectional view showing relative positions of the lipid acyl chains (thin irregular lines), the lipid headgroup region (dark bars above and below the acyl chains), and two helices on either edge. The dense circle in the center of each helix represents the diameter of the main chain atom coil, while the lighter region around each coil represents the extent of the amino acid side chains.

measure lipid-induced changes in the electrostatic microenvironment of the receptor-binding region (*20*−*22*).

In this investigation, synthetic lipoprotein particles were prepared with each of the full-length apoE isoforms, as well as with the truncated N-terminal and C-terminal domains. These particles were examined with calorimetry, electron microscopy, circular dichroism spectroscopy, and polarized attenuated total internal reflection Fourier transform infrared spectroscopy (PATIR-FTIR). In a previously published study, the latter technique proved to be valuable in establishing the structure of lipoprotein A-I (LpA-I) (*23*), a 243-amino acid protein that is 44% similar in sequence to apoE, and has a similar pattern of 11- and 22-amino acid tandem repeat sequences (*24*−*26*). These studies concluded that the lipid molecules in LpA-I are organized as a flat bilayer, and that the apoA-I α-helices wrap around the circumference of the bilayer. This constitutes the "belt model" of LpA-I structure (Figure 1). Because this model has become generally accepted, parallel studies were performed on both apoE and apoA-I in this investigation.

EXPERIMENTAL PROCEDURES

Materials. 1,2-Dimyristoyl-*sn*-glycero-3-phosphocholine (DMPC, di-14:0 PC), 1,2-dimyristoyl-*sn*-glycero-3-phosphoserine (DMPS, di-14:0 PS), 1,2-dipalmitoyl-*sn*-glycero-3-phosphocholine (DPPC, di-16:0 PC), 1,2-dipalmitoyl-*sn*-glycero-3-phosphoserine (DPPS, di-16:0 PS), 1-palmitoyl-2-oleoyl-*sn*-glycero-3-phosphocholine (POPC, 16:0,18:1 PC), and 1-palmitoyl-2-oleoyl-*sn*-glycero-3-phosphoserine (POPS, 16:0,18:1 PS) were purchased from Avanti Polar Lipids (Alabaster, AL), and stock solutions were stored in a chloroform/methanol (2/1) mixture under nitrogen at −20 °C. Their purities were assayed by thin-layer chromatography on silica gel G plates (Analtech, Newark, DE) in a chloroform/methanol/water (65/25/4, v/v) mixture. Lipids were visualized by spraying developed thin layer plates with a 50% sulfuric acid solution and charring at 200 °C for 15 min. D_2O (Cambridge Isotope Laboratories, Andover, MA) was routinely deoxygenated and stored under nitrogen.

Bacteriological media were obtained from Fisher (Pittsburgh, PA). The pET32a prokaryotic expression vector was from Novagen (Madison, WI), and competent *Escherichia coli* strain BL21-DE3 was from Invitrogen (Carlsbad, CA). Competent *E. coli* strain DH5α was from Life Technologies (Gaithersburg, MD). PCR supplies were from Qiagen (Chatsworth, CA). Restriction enzymes were purchased from Promega (Madison, WI). Isopropyl β-D-thiogalactopyranoside, β-mercaptoethanol, aprotinin, and ampicillin were from Sigma. Ultrapure guanidine HCl was from ICN Pharmaceuticals (Costa Mesa, CA). Oligonucleotides were from IDT (Coraville, IA), and DNA purification kits were from Qiagen.

Expression and Purification of Proteins. Full-length human apoE2, apoE3, apoE4, and the 22 and 10 kDa fragments of apoE3 were expressed in *E. coli* and purified as described previously (*27*−*29*). The 22 kDa fragment consists of residues 1−191 of full-length apoE3, and includes the mutation sites at positions 112 and 158. The 10 kDa fragment consists of residues 222−299 and is the same in all the isoforms (*7*). Further purification beyond 95% was achieved by subjecting the proteins to gel filtration on a Superdex 75 column.

Preparation of ApoE·DMPC/DMPS Particles. DMPC (45 mg) and DMPS (5 mg) were mixed and dried from a chloroform/methanol (2/1, v/v) solution under nitrogen to a thin film on the walls of a 15 mL glass (Corex) tube and lyophilized overnight to remove any remaining organic solvents. The lipids were rehydrated in 10 mL of TBS buffer [150 mM NaCl, 1 mM disodium EDTA, and 10 mM Tris-HCl (pH 7.6)] for at least 30 min at room temperature and vortexed gently every 10 min and then sonicated for 45 min at 24 or 45 °C in a Branson 350 sonicator fitted with a tapered tip (5 min on, 2 min off). The mixture was then centrifuged at low speed to remove titanium released from the sonicator tip. The slightly translucent solution of DMPC/DMPS vesicles was kept at room temperature. ApoE samples (full-length apoE2, -E3, and -E4 proteins and the 22 and 10 kDa fragments of apoE3) were dissolved in 6 M guanidine HCl, allowed to sit overnight at 4 °C, dialyzed against 0.1 M NH_4HCO_3 (pH 8.1) to a final concentration of 2 mg of protein/mL, and then pipetted into plastic tubes. Intermolecular disulfide bonds were reduced by a 30 min incubation at room temperature with β-mercaptoethanol (0.5 μL/100 μg of protein). DMPC/DMPS vesicles were added to the protein solutions, and the mixtures were recycled three times through the gel−liquid crystal transition temperature of the DMPC/DMPS mixture by warming to ∼45 °C and cooling to ∼15 °C, and then dialyzed extensively against TBS buffer. The complexes were separated from the uncomplexed proteins and lipids by gel filtration chromatography using a calibrated Superdex 200 Prepgrade column in a fast protein liquid chromatography system. The elution profile closely resembled those described previously such that the elution fraction partition coefficient (K_{av}) of LpE-FL is 0.25. This is similar to the coefficient of 0.20 for LpA-I (*30*). In addition, the K_{av} of free apoE was 0.5, which is identical to that of free apoA-I. Fractions (1 mL) were collected, and the absorbance of each fraction was monitored at 280 nm to locate the protein peaks. The hydrodynamic diameters of the particles were calculated from the elution volume, as described previously (*30*). Fractions containing the complexes were pooled and dialyzed against saline-EDTA before characterization.

Preparation of ApoE·POPC/POPS and ApoE·DPPC/DPPS Particles. Lipoprotein particles were prepared by the cholate dispersion/Biobead removal technique as described previously (*31*). For DPPC/DPPS particles, the incubation temperature was 41 °C instead of 37 °C. The complexes were separated from the uncomplexed proteins and lipids by gel

Table 1: Physical Characteristics of DMPC/DMPS/Apolipoprotein Discoidal Lipoprotein Particles[a]

lipoprotein variant	lipid/protein ratio (w/w)[b]	radius (Å)[c]	helicity (%)[d]	no. of lipid molecules per particle[e]	no. of protein molecules per particle[e]
LpE2-FL	0.9/1	52	73	170	4
LpE3-FL	0.9/1	54	75	185	4
LpE4-FL	0.9/1	53	74	180	4
LpE-TD_{10}	3.5/1	54	75	280	6
LpE3-TD_{22}	3.0/1	52	73	290	3
LpA-I-FL	1.8/1	52	69	260	3

[a] Particle lipid composition is 90% DMPC and 10% DMPS. [b] Composition of the peak that contains lipid−protein discoidal complexes. [c] Hydrodynamic radius calculated from gel filtration chromatography elution volumes. [d] Percentage α-helix determined from molar ellipticities at 222 nm (±5%). [e] Determined from particle volume and density calculations assuming a cylindrical model.

filtration chromatography as for DMPC/DMPS lipoprotein particles.

Analytical Procedures. Protein concentrations were determined by the procedure of Lowry and co-workers (*32*) or absorbance at 280 nm (extinction coefficient of 44 460 M^{-1} cm^{-1}). Phospholipid concentrations were determined by the phosphorus analysis procedure of Bartlett (*33*). The concentrations determined by these analytical procedures were used to determine the lipid/protein mass ratios of the lipoprotein particles after gel filtration chromatography. Polyacrylamide gel electrophoresis (8 to 25% gradient) in the presence of SDS was performed with an Amersham Pharmacia Biotech Phast electrophoresis system to monitor the purity of the proteins.

Calculations. The number of molecules of lipid and protein per particle was determined by modeling each particle type as a cylinder with a height of 45 Å, corresponding to the thickness of the hydrophobic portion of a DMPC bilayer (*34*), and a radius assigned according to the measured hydrodynamic radii. The simple geometry of this model enables one to calculate a particle volume, $vol_{particle}$, which in turn is equated to $m_P\bar{v}_P + m_L\bar{v}_L$, where partial specific volumes were assumed to be 0.971 mL/g for lipid ($\bar{v}_L$) and 0.714 mL/g for protein ($\bar{v}_P$) and the ratio, r, of the measured lipid and protein concentrations for each particle type is equated to the ratio of lipid and protein masses per particle ($r = m_P/m_L$). Thus, there are two simultaneous equations from which m_P and m_L may be calculated and converted to the number of protein and lipid molecules per particle.

The amphipathic portion of each protein was assumed to be α-helical (see Table 1) (*35*) and capable of covering a 14 Å wide hydrophobic strip around the perimeter of a lipid bilayer. Given the number of amino acid residues in the protein (Table 2), the fraction that is α-helical (Table 1), and the number of protein molecules per particle (Table 1), the amount of hydrophobic protein surface area per particle was calculated (Table 2). Likewise, assuming that the edge of the lipid bilayer is 40 Å wide, and that each lipid molecule occupies 45 $Å^2$ on either surface of the bilayer (*36*), the area and circumference for the bilayer disk and the amount of hydrophobic surface area around the perimeter of the bilayer were calculated (Table 2). Finally, the ratio between the lipid and protein hydrophobic surface areas was calculated to facilitate comparison between particles.

Negative Staining Electron Microscopy (EM). LpE3-FL and LpE3-TD_{22} containing 10% DMPS and 90% DMPC were prepared for electron microscopy by dialysis against 125 mM NH_4CH_3COO and 2.6 mM NH_4HCO_3. Electron microscopy with negative staining was used to measure the size of the lipoprotein particles as described previously (*37*).

Quasi-Elastic/Dynamic Light Scattering (DLS). LpE3-FL and LpE3-TD_{22} containing 10% DMPS and 90% DMPC were diluted to 20 μg/mL into filtered buffer. The hydrodynamic radius was measured at 20 °C with a 10 s acquisition time on a Protein Solutions DynaPro model 99E instrument with a 825 nm laser. The results were analyzed using Dynamics 3.14 software from Proterion using a Rayleigh sphere model.

Circular Dichroism (CD) Spectroscopy. The protein secondary structure in lipoprotein complexes was assessed at room temperature using a Jasco J-600 spectropolarimeter. The complexes were dialyzed overnight against excess 10 mM sodium phosphate buffer (pH 7.4) and diluted to 25−50 μg of protein/mL. The α-helix contents were calculated as described previously (*24*) assuming that a molar ellipticity of −39000 deg cm^2 $dmol^{-2}$ at 222 nm corresponds to 100% α-helix. A multicomponent fit of the spectra across the entire wavelength range was not possible because of interference due to lipid below 208 nm.

Differential Scanning Calorimetry (DSC). Heat capacity profiles of degassed samples of lipid mixtures and lipid−protein complexes (1.0−3.5 mg of lipid/mL) were determined over a temperature range of 10−50 °C with a high-resolution differential scanning calorimeter (MCS, MicroCal, Amherst, MA). The calorimeter was calibrated with heat pulses and temperature standards supplied by the manufacturer as outlined in the user manual. Endotherms were typically recorded at a scan rate of 1 °C/min. Baseline runs with buffer-filled cells preceded each sample run. Buffer−buffer references were subtracted from sample data, and the data were normalized to protein concentrations. Progress baselines were generated and subtracted from the data, which

Table 2: Physical Characteristics of Discoidal Lipoprotein Particles[a]

lipoprotein variant	no. of residues per protein	no. of helical residues per particle[b]	protein surface area ($Å^2$)[c]	lipid disk circumference (Å)	lipid surface area ($Å^2$)[d]	lipid/protein surface area ratio[e]
LpE2-FL	299	873	13096	219	6577	0.50
LpE3-FL	299	897	13455	229	6861	0.51
LpE4-FL	299	885	13276	226	6768	0.51
LpE-TD_{10}	84	378	5670	281	8441	1.49
LpE3-TD_{22}	191	418	6274	286	8590	1.37
LpA-I-FL	243	503	7545	271	8134	1.08

[a] All calculations assume a cylindrical model and a lipid composition of 90% DMPC and 10% DMPS. [b] The number of residues per protein × the number protein molecules per particle × helicity. [c] The number of helical residues per particle × 1.5 Å helix length per residue × 14 Å helix diameter. [d] (Number of lipid molecules per particle/2 × 45 $Å^2$ per lipid molecule × $4\pi)^{1/2}$. [e] Lipid surface area/protein surface area.

were then analyzed using the Microcal ORIGIN software package. Heat capacity curves for the lipids complexed with the apoE proteins were deconvoluted according to a two-state model.

Infrared Spectroscopy. Polarized attenuated total internal reflection Fourier transform infrared (PATIR-FTIR) spectroscopy was performed using a Bio-Rad FTS-6000 spectrometer equipped with a liquid nitrogen-cooled MCT detector and coupled to a lipid film balance. Lipid monolayers composed of 80 mol % DMPC and 20 mol % DMPS were spread at room temperature at the air−water interface in the film balance, compressed to a surface pressure of 20 dyn/cm, and applied to an octadecyltrichlorosilane-treated germanium crystal by placing the crystal flat onto the monolayer (*38*, *39*).

Polarized infrared absorption spectra were recorded by directing light from the FTIR spectrometer through a BaF_2 polarizer oriented either parallel or perpendicular to the plane of the incident beam of light, into the crystal at an angle of 30° from a normal to the crystal surface. After a series of internal reflections, the beam exits the crystal and is directed into an external detector (*40*). All spectra were collected in the rapid scan mode as 1024 co-added interferograms, with a resolution of 2 cm^{-1}, a scanning speed of 20 MHz, triangular apodization, and one level of zero filling. Baseline spectra were recorded immediately prior to the addition of 8 μg of protein in lipoprotein complexes to the continuously stirred buffer subphase composed of 30 mM HEPES and 1 mM $CaCl_2$ in D_2O at pD 7.4.

When calcium in the buffer is replaced with a calcium chelator, there is no absorption signal. This demonstrates that only lipoprotein complexes in the subphase that were in contact with the lipid monolayer on the crystal attenuate the evanescent field created by each internal reflection and contribute to the absorption spectrum, and suggests that calcium ions form bridges between the seryl headgroups in the monolayers and in the lipoprotein particles. The presence of 20 mol % DMPS in the monolayer, and only 10 mol % DMPS in the lipoprotein particles, renders monolayer−particle interactions stronger than particle−particle interactions in the presence of Ca^{2+} ions. The instrument is designed so that any particles that do aggregate in the presence of Ca^{2+} will be pulled away from the monolayer by gravity.

From the polarized absorption spectra, dichroic ratios ($R_z = \int A_{||}/\int A_{\perp}$) were evaluated using integrated areas of characteristic absorption bands, $\int A$, as determined by simultaneous linked analysis of sets of parallel and perpendicular spectra (*39*). Dichroic ratios were converted to order parameters, $S(R_z)$, using the equation

$$S(R_z) = \frac{\langle E_x^2\rangle - R_z\langle E_y^2\rangle + \langle E_z^2\rangle}{\langle E_x^2\rangle - R_z\langle E_y^2\rangle - 2\langle E_z^2\rangle} \qquad (2)$$

and mean electric field amplitude components $\langle E_x\rangle$, $\langle E_y\rangle$, and $\langle E_z\rangle$ were calculated using the two-phase approximation (*41*, *42*). An order parameter S of 1.0 indicates a uniform orientation perpendicular to the membrane surface, while a value of −0.5 indicates a uniform orientation parallel to the membrane. An order parameter of 0.0 may indicate either a uniform orientation at the magic angle ($\theta = 54.7°$ relative to the membrane normal), complete disorder as in an isotropic system, or any other orientation distribution for which $\langle \cos^2\theta\rangle = {}^1/_3$. An order parameter S of −0.45 is the most negative value that can be measured with this technique due to surface imperfections in the germanium internal reflection crystal (*40*).

RESULTS

Physical Characterization of Lipoprotein Particles. During particle preparation, lipid/protein ratios were adjusted to produce particles with a hydrodynamic radius of 52−54 Å, and subjected to gel filtration chromatography to obtain particles of uniform size and to remove uncomplexed lipid and protein. To compare the basic physical characteristics of these particles, their composition and α-helical content were determined. The three isoforms of LpE-FL each had an average lipid to protein mass ratio of 0.9 (Table 1); this ratio was 2-fold higher for LpA-I and more than 3-fold higher for both types of LpE-TD. CD spectroscopy indicated that apoE was 70−75% α-helical in all particle types.

To estimate the number of lipid and protein molecules per particle, LpE-FL isoforms, LpE-TD_{10}, and LpE3-TD_{22} were modeled as cylinders with radii of 52−54 Å (the measured hydrodynamic radius) and heights of 42−48 Å (the thickness of a typical DMPC bilayer). According to eq 1, LpE-FL with these dimensions should contain four protein and 180 lipid molecules (Table 1). A different geometric model used to approximate particle shape yields similar results (see the Supporting Information).

This information permits us to test the plausibility of the belt model (*23*, *43*) for LpE structure (Figure 1). The geometric calculations detailed in Experimental Procedures, and the results summarized in Tables 1 and 2, indicate that the area of a hydrophobic strip around the perimeter of a flat lipid disk, and the hydrophobic portion of an α-helical protein surface, are approximately equal for LpA-I. This equivalence is expected in the belt model because the hydrophobic aspect of the amphiphilic α-helix presumably stabilizes the perimeter of the bilayer. In comparison, LpE-FL particles are deficient in lipid, and LpE-TD particles have an excess of lipid. Assuming that LpA-I particles conform to the belt model of lipoprotein structure, these calculations suggest that none of the LpE particle types conform to this simple model.

EM and DLS. To complement chromatographic measurements of hydrodynamic radius, electron microscopy (EM) and dynamic (quasi-elastic) light scattering (DLS) were used to characterize lipoprotein particle size. Like several other types of lipoprotein particles (*44*), LpE particles stack to form rouleaux when dehydrated under low-salt conditions (Figure 2). Such rouleaux formation is consistent with that observed for discoidal lipoprotein particles of DMPC and human full-length apoE isolated from plasma (*45*). Electron micrographs of negatively stained rouleaux provide rough estimates of particle diameter, but enable relatively precise estimates of average particle thickness from measurements of rouleaux stack length and a count of the number of particles in the stack.

LpE3-FL and LpE3-TD_{22} both appear to have an outer radius of 53 Å (Table 3). This result agrees with the hydrodynamic radii measured by gel filtration chromatography. LpE3-FL are 60 Å thick, while LpE3-TD_{22} are ∼5 Å

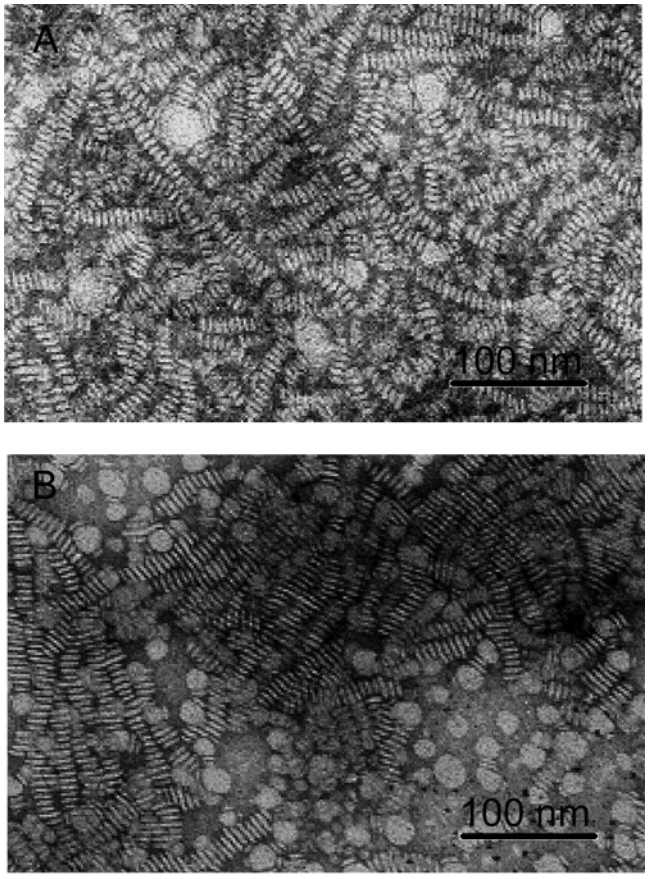

FIGURE 2: Negatively stained scanning electron microscopy of rouleaux formed by (A) LpE3-FL and (B) LpE3-TD_{22} particles.

Table 3: Electron Microscopy and Dynamic Light Scattering

lipoprotein variant	EM radius (Å)	EM thickness (Å)	DLS radius (Å)
LpE3-FL[a]	53 ± 9	60 ± 4	74 ± 8
LpE3-TD_{22}[b]	53 ± 6	55 ± 5	71 ± 1

[a] Lipid composition: apoE3 with 10% DMPS and 90% DMPC. [b] Lipid composition: apoE3-22 with 10% DMPS and 90% DMPC.

thinner. These dimensions correspond well to the 58.5 Å thickness of a DMPC bilayer in the $P_{\beta'}$ phase (*46*). DLS estimates of particle size are larger than those obtained by gel filtration and electron microscopy. However, these estimates are susceptible to overestimation due to particle aggregation, so the results should be viewed as upper limits, not precise measurements.

DSC of Lipid Mixtures and Lipid−Protein Complexes. To characterize the effect of the protein component on lipid bilayer properties, thermal phase transitions were examined with DSC (Table 4). Multilamellar DMPC vesicles exhibit a very narrow thermal transition at 23.9 °C, while DMPS vesicles undergo a slightly wider transition at 40.8 °C. Vesicles made from a 9/1 DMPC/DMPS mixture exhibit a biphasic transition at a temperature only slightly higher than that of pure DMPC vesicles. There is no evidence of this transition in lipoprotein particles made with the same lipid mixture and apoE3 (LpE3-FL), however. The transitions in both types of LpE-TD are much narrower than LpE3-FL (Figure 3), and the transition is closer in temperature to that of pure lipid vesicles. Full-length apoE3 in particles made with POPC has been previously shown to exhibit a transition at a temperature greater than 60 °C (*47*). Therefore, it is

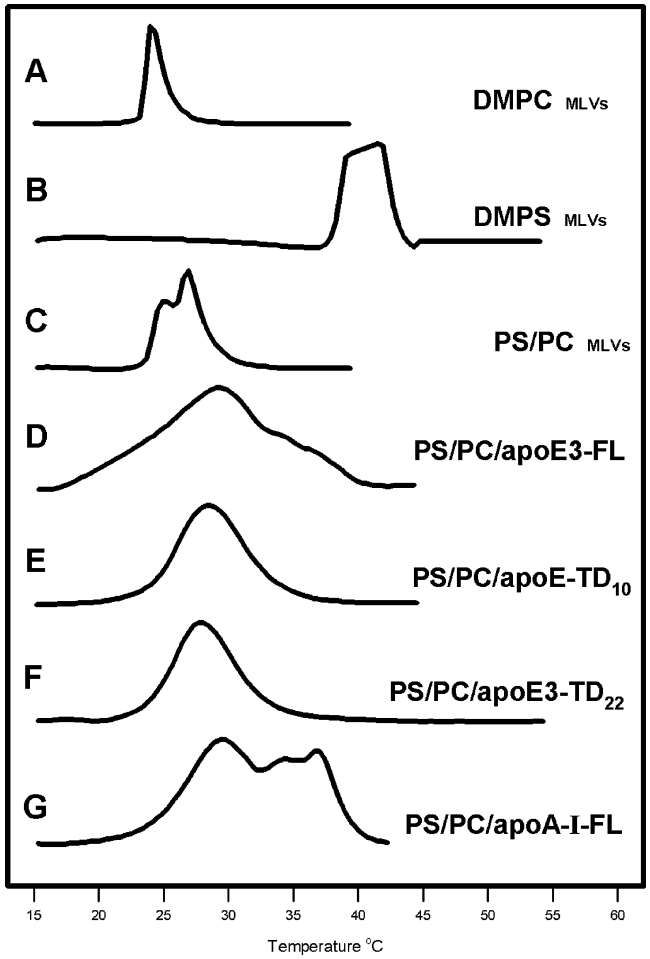

FIGURE 3: Differential scanning calorimetry of (A) DMPC MLV, (B) DMPS MLV, (C) 10% DMPS/90% DMPC MLV, (D) 10% DMPS/90% DMPC/apoE3-FL, (E) 10% DMPS/90% DMPC/apoE-TD_{10}, (F) 10% DMPS/90% DMPC/apoE3-TD_{22}, and (G) 10% DMPS/90% DMPC/apoA-I-FL.

Table 4: Phase Transition Temperatures of DMPC/DMPS Mixtures and Apolipoprotein−Lipid Complexes[a]

preparation	beginning[b]	T_{m1}	T_{m2}	T_{m3}	end[b]	ΔH
DMPC MLV	19.5		23.9 ± 0.1		31.2	7.2 ± 0.6
DMPS MLV	37.6		40.8 ± 0.1		43.8	8.8 ± 1.1
9/1 PC/PS MLV	21.6	25.4 ± 0.1	27.0 ± 0.1		34.5	7.5 ± 0.3
LpE-TD_{10}[c]	19.9		28.2 ± 0.2		40.0	4.4 ± 0.4
LpE3-TD_{22}[c]	20.0		28.2 ± 0.02		40.1	2.4 ± 0.2
LpE3-FL[c]	17.4	29.6 ± 0.2	33.0 ± 0.5	36.1 ± 0.2	41.4	5.0 ± 0.7
LpA-I-FL[c]	21.6	29.7 ± 0.2	33.0 ± 0.2	36.5 ± 0.2	40.9	3.4 ± 0.4

[a] T_m measurements in degrees Celsius; phase transition enthalpies in kilocalories per mole of phospholipid. [b] These temperatures are accurate to within ±0.2 °C. [c] All complexes were made with a 9/1 DMPC/DMPS weight ratio.

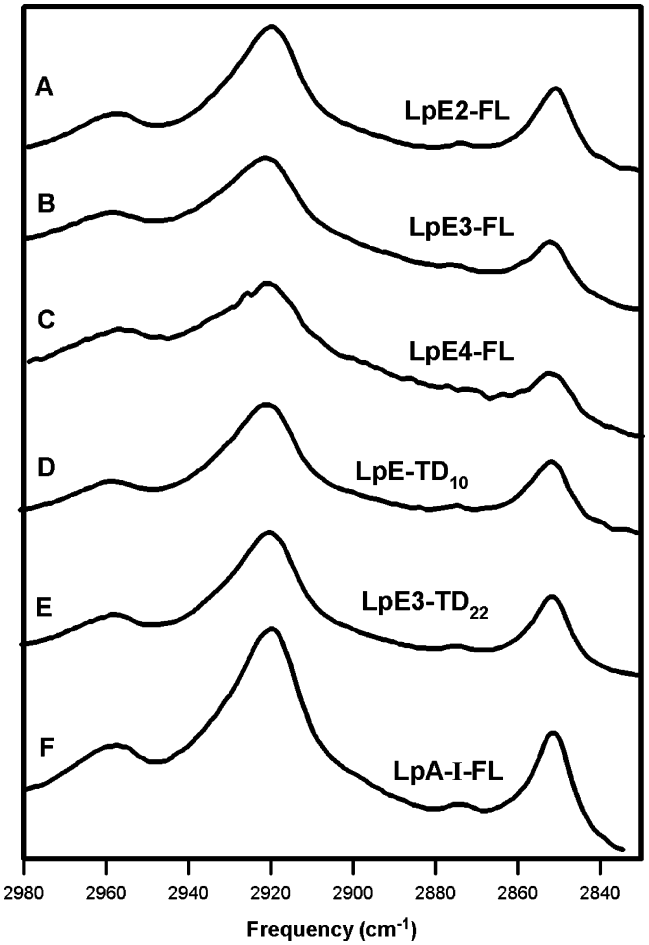

FIGURE 4: Infrared spectra of lipid methylene stretching regions of (A) LpE2-FL, (B) LpE3-FL, (C) LpE4-FL, (D) LpE-TD_{10}, (E) LpE3-TD_{22}, and (F) LpA-I-FL.

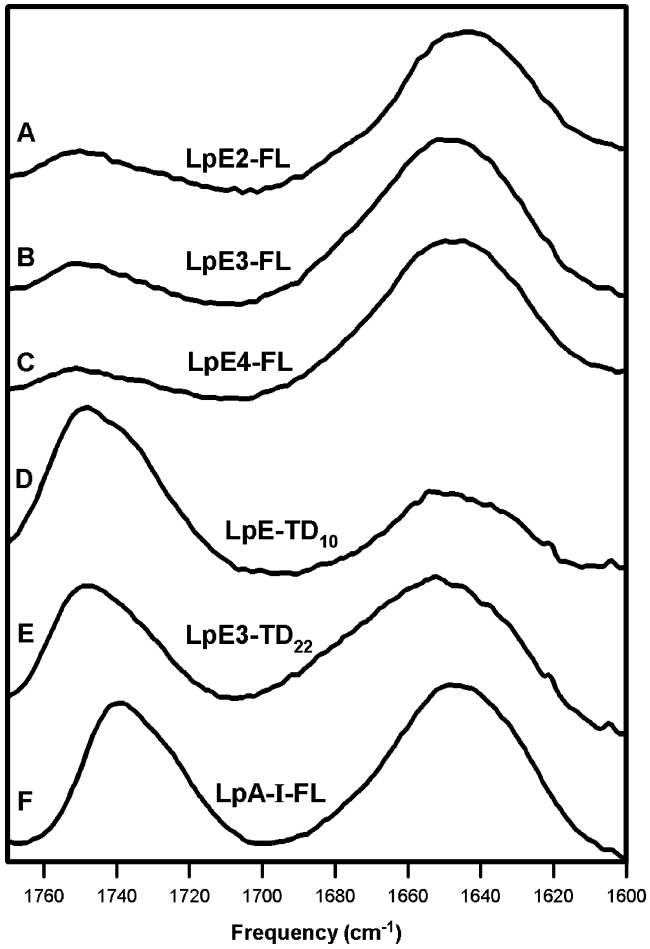

FIGURE 5: Infrared spectra of lipid ester and amide I regions of (A) LpE2-FL, (B) LpE3-FL, (C) LpE4-FL, (D) LpE-TD_{10}, (E) LpE3-TD_{22}, and (F) LpA-I-FL.

unlikely that thermal transitions arising from protein overlap with transitions arising from lipid in our experiments. LpA-I exhibit multiple partially resolved transitions at temperatures intermediate between that of DMPC and DMPS vesicles.

Vibrational Spectroscopy: Particle Composition. Internal reflection infrared spectroscopy was used to characterize lipid/protein ratios, protein conformation, and the orientations of lipid and protein components in LpE. Lipid methylene group absorptions were nearly identical in shape and intensity for all LpE-FL isoforms and LpE-TDs (Figure 4). Lipid ester carbonyl group absorptions at 1720−1760 cm^{-1}, however, differ among the particles, particularly in comparison to the amide I group absorptions at 1620−1680 cm^{-1} (Figure 5). Gross visual comparison of the ester/amide I band area ratios suggests that LpE-TD_{10} has a higher and the three LpE-FL isoforms have a lower lipid/protein ratio than LpA-I. This pattern is consistent with the measured lipid/protein ratios listed in Table 1. LpE3-TD_{22} is somewhat anomalous in this regard, with an ester/amide band area ratio that resembles that of LpA-I, but a measured lipid/protein ratio that is the same as that of LpE-TD_{10}. This discrepancy may arise from differences in sample orientation (see below) within the evanescent field, rather than true differences in lipid and protein content.

Vibrational spectroscopy: Protein Conformation. To assess differences in the conformation and orientation of the protein and lipid components among the lipoprotein particles, parallel and perpendicularly polarized spectra were quantitatively analyzed using linked analysis (*39*). Results of the amide I analysis are illustrated in Figure 6, and listed in Tables 5−7. The three LpE-FL isoforms yielded virtually identical spectra. In each case, the dominant amide I component was located at 1648.8 cm^{-1}, with smaller components at 1631.4 and 1672.7 cm^{-1} (Table 5). The location of the dominant amide I component is consistent with the CD results indicating a largely α-helical secondary structure, although the infrared spectra clearly suggest that other secondary structures are also likely to be present. Compared to LpE-FL, LpE3-TD_{22} had more absorption at high frequency, 1672.3 cm^{-1}, whereas LpE-TD_{10} had less. Thus, if one added the amide I spectra from the two fragments together, it would yield a spectrum similar to that obtained from the LpE-FL isoforms.

Vibrational Spectroscopy: Component Orientations. The three isoforms of LpE-FL are virtually indistinguishable with respect to the orientational order of their protein and lipid components. Negative order parameters indicate that the vibrational transition moment orientations for peptide groups, lipid ester carbonyl groups, and lipid methylene groups are all preferentially oriented parallel to the surface on which they are supported (Table 6), and the lipid acyl chains are oriented perpendicular to the surface. However, the degree of orientational order for lipid acyl chains in LpE-FL is significantly lower than that of LpΔ(1−43)A-I (i.e., order

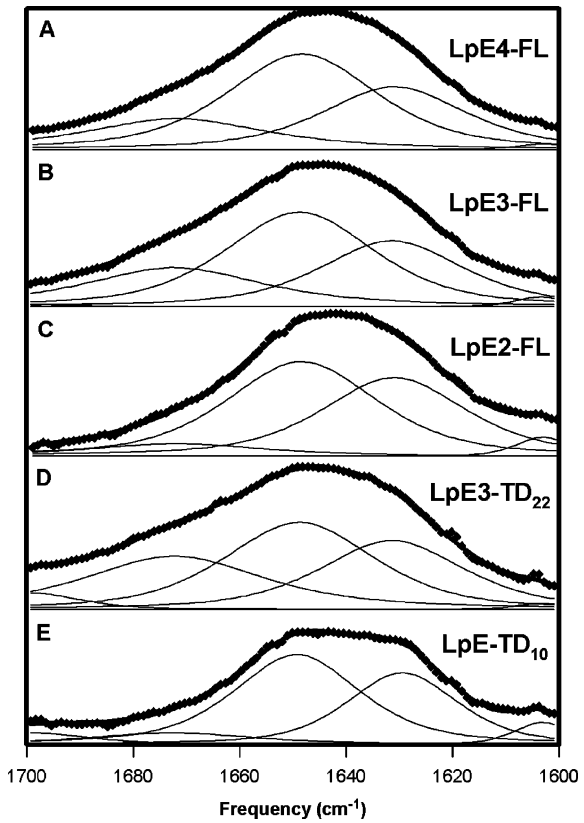

FIGURE 6: Results of simultaneous fitting of infrared amide I spectra using linked band shape analysis (*39*) for (A) LpE4-FL, (B) LpE3-FL, (C) LpE2-FL, (D) LpE3-TD_{22}, and (E) LpE-TD_{10}.

parameters are closer to zero), suggesting that the structure of LpE-FL is at some variance with the belt model for discoidal particles of LpΔ(1−43)A-I (Figure 1). Amide I order parameters in LpE-FL are similar to that of LpA-I-FL.The latter includes 43 N-terminal residues believed to be disordered.

Table 7: Order Parameters, $S(R_z)$, Obtained for the Complexes of ApoE Isoforms with Different Phospholipid Acyl Chain Compositions[a]

lipoprotein variant	amide I (overall)	symmetric CH_2 stretch (~2852 cm^{-1})
LpE3-FL POPC[b]	−0.19 ± 0.02	−0.32 ± 0.04
LpE4-FL POPC[b]	−0.22 ± 0.02	−0.32 ± 0.01
LpE4-FL DPPC[c]	−0.15 ± 0.01	−0.40 ± 0.01

[a] Data reported are the mean values of $S(R_z)$ ± the mean deviation of results from at least three measurements. [b] Lipid composition: 10% POPS and 90% POPC. [c] Lipid composition: 10% DPPS and 90% DPPC.

Lipid order in LpE-TD was similar to that in LpE-FL, but the level of amide I order tended to be higher, particularly for the low-frequency amide I component in LpE-TD_{10}. This suggests that the secondary structure and orientation of the protein component in LpE-TD_{10} are relatively homogeneous compared to those of the LpE-FL isoforms. Changing the lipid component acyl chains from fully saturated (di-14:0) to longer and monounsaturated acyl chains (16:0, 18:1) did not significantly alter the protein or lipid order, but merely lengthening the acyl chains (to di-16:0) increased the lipid order significantly, while slightly decreasing the protein order (Table 7). The increased orientational order for lipid acyl chains in particles made with di-16:0 lipids is expected because the lipid is likely to be below its phase transition temperature. Reduced order for the protein component in these same particles is not surprising because the exposed hydrophobic surface area of the lipid is greater without a corresponding increase in the hydrophobic surface of the protein, and one would expect less well-defined protein−lipid relationships under these conditions.

DISCUSSION

Compelling evidence indicates that LpA-I conforms to a double-belt or hairpin-belt model of lipoprotein structure

Table 5: IR Fit Data for ApoE−DMPC/DMPS Complexes[a]

frequency (cm^{-1})	width (cm^{-1})	shape (%)[b]	LpE2-FL	LpE3-FL	LpE4-FL	LpE-TD_{10}	LpE3-TD_{22}
1603.1	12.5	44.1	1.6 ± 1.2	0.7 ± 0.1	1.1 ± 1.1	1.8 ± 0.6	0.5 ± 0.2
1629.4	24.6	48.4				38.5 ± 9.7	
1631.4	34.2		36.4 ± 7.2	30.4 ± 1.1	31.9 ± 8.6		30.3 ± 7.4
1648.8	28.1	43.0				48.3 ± 3.0	
	34.3		50.2 ± 5.9	47.4 ± 1.1	47.3 ± 2.6		39.7 ± 1.7
1672.7	38.0	24.4	10.3 ± 5.5	21.3 ± 1.7	18.5 ± 11.5	7.8 ± 6.1	26.6 ± 9.1
1699.3	27.3	51.9	1.4 ± 2.3	0.3 ± 0.3	1.2 ± 1.6	3.5 ± 1.2	2.9 ± 0.4

[a] Results are the average percent of the 1700−1600 cm^{-1} signal with the standard deviation for three experiments (six polarized spectra). [b] Shape (%) = % Gaussian vs Lorentzian.

Table 6: Order Parameters, $S(R_z)$, Obtained for the DMPC/DMPS Complexes of ApoE Isoforms and ApoE Fragments[a]

lipoprotein variant	amide I (1629−1632 cm^{-1})	amide I (1648.8 cm^{-1})	amide I (overall)	symmetric CH_2 stretch (~2852 cm^{-1})
LpE2-FL	−0.24 ± 0.06	−0.11 ± 0.01	−0.19 ± 0.01	−0.32 ± 0.02
LpE3-FL	−0.21 ± 0.00	−0.12 ± 0.01	−0.17 ± 0.03	−0.32 ± 0.02
LpE4-FL	−0.24 ± 0.05	−0.13 ± 0.04	−0.18 ± 0.01	−0.33 ± 0.01
LpE-TD_{10}	−0.34 ± 0.02	−0.13 ± 0.04	−0.23 ± 0.04	−0.33 ± 0.06
LpE3-TD_{22}	−0.29 ± 0.03	−0.15 ± 0.02	−0.19 ± 0.03	−0.32 ± 0.03
LpA-I-FL[b]	NM[c]	NM[c]	−0.19 ± 0.04	−0.43 ± 0.05
LpΔ(1−43)A-I[b]	NM[c]	NM[c]	−0.28 ± 0.02	−0.45 ± 0.01

[a] Data reported are the mean values of $S(R_z)$ ± the mean deviation of results from at least three measurements. [b] The data listed have been previously published (*23*). They were obtained on a version of the PATIR-FTIR instrument in which the internal reflection crystal end-facets are at a 45° angle to the surface normal, but results for the symmetric CH_2 stretch order in LpA-I-FL have been reproduced on the current instrument in which the end-facets are at a 60° angle. [c] Not measured.

(Figure 1) (*23*, *25*, *26*, *48*−*52*), but two independent sets of results reported herein indicate that LpE does not conform to this model. First, calculations indicating that hydrophobic protein and lipid surface areas in LpA-I-FL are approximately equal and therefore consistent with the belt model also indicate that LpE-FL have an excess of protein, while LpE-TD have an excess of lipid, and are therefore inconsistent with this model. Second, the PATIR-FTIR results for lipid orientational order (symmetric CH_2 stretch, Table 6) indicate that lipid acyl chains in LpE are significantly less ordered than in LpA-I. Previous studies of LpE using PATIR-FTIR agree in general with our conclusion that the protein component is oriented perpendicular to acyl chains of the lipid component (*53*); however, the results of that study are not truly comparable because they were obtained from dried lipoprotein samples, and by applying a different set of technical assumptions (*23*).

The data presented herein may be used to evaluate various models of LpE structure. The order parameter measured for the lipid acyl chains of LpE-FL and LpE-TD ($S = -0.32$) indicates that they are neither flat like LpA-I ($S = -0.45$) nor spherical ($S = 0.00$). An oblate ellipsoid 85 Å thick at the center and 45 Å thick at the perimeter (the thickness of DMPC in the liquid crystalline phase), with a radius of 52 Å, would yield an order parameter with this value (see Figure 7A and Supporting Information). However, it is not clear how either the lipid or the protein components in LpE might be configured to occupy and stabilize the hydrophobic cavity that would have to exist in the center of such an ellipsoid. Moreover, the EM images reveal that the thickness of LpE3-FL corresponds to the thickness of a bilayer, not an oblate ellipsoid.

The EM and DSC data both support the presence of bilayer structure in LpE, suggesting that the reduced lipid acyl chain disorder observed by PATIR-FTIR is not due to bilayer curvature but another type of perturbation. For example, well-ordered lipids in a bilayer may appear to have less order if they assume a tilted orientation on the internal reflection crystal surface (Figure 7B), and a 26° tilt would account for a reduction in acyl chain order from −0.45 to −0.32. The hydrophobic surface area calculations indicate that LpE-FL have an "excess" of protein available for lipid−protein interaction compared to the lipid component, and this protein may prevent flat adsorption of the bilayer on the support surface. Again, however, the EM studies indicate that nothing prevents LpE-FL from lying flat on a surface, and this model is unable to explain why LpE-TD yield the same acyl chain order parameters as LpE-FL while they contain an excess of lipid, not of protein.

Therefore, the model which best fits all of the data is a previously suggested modification of the belt model in which amphipathic α-helices not only encircle a lipid bilayer like a belt but also lie horizontally within the interfacial region of the lipid bilayer (*54*) (Figure 7C). This modified belt model would account for the excess hydrophobic protein surface area compared to lipid, and for the DSC results suggesting more extensive lipid−protein interactions in LpE-FL. Moreover, in this model, embedded α-helices would perturb adjacent lipid acyl chains, accounting for their reduced orientational order.

Since there is not enough hydrophobic protein surface to stabilize the hydrophobic surface around the perimeter of a lipid bilayer disk in LpE-TD (Table 2), these particles must assume a configuration different from that of LpE-FL. Possible configurations include a single-helix belt (Figure 7D, left) or a micelle-like edge, perhaps stabilized by protein (Figure 7D, right). Either of these configurations would account for the reduced acyl chain order of lipids in LpE-TD (relative to that of LpA-I). However, these structures imply that the similarity of acyl chain order in LpE-FL and LpE-TD is coincidental. Although both are reduced to the same degree relative to LpA-I, the physical basis for the reduction differs. The calorimetry data (Figure 3 and Table 4) are important in this regard, since they indicate that the lipid component in both types of LpE-TD undergoes cooperative transitions, but that the molar enthalpies of these transitions are reduced relative to that of LpE-FL, especially in LpE3-TD_{22}. Therefore, these data support our conclusion that a smaller fraction of total lipid in LpE-TD is perturbed by protein−lipid interactions, or involved in nonbilayer structure, than in LpE-FL. The calorimetry data are also consistent with the much higher lipid/protein ratios in both types of LpE-TD than in LpE-FL.

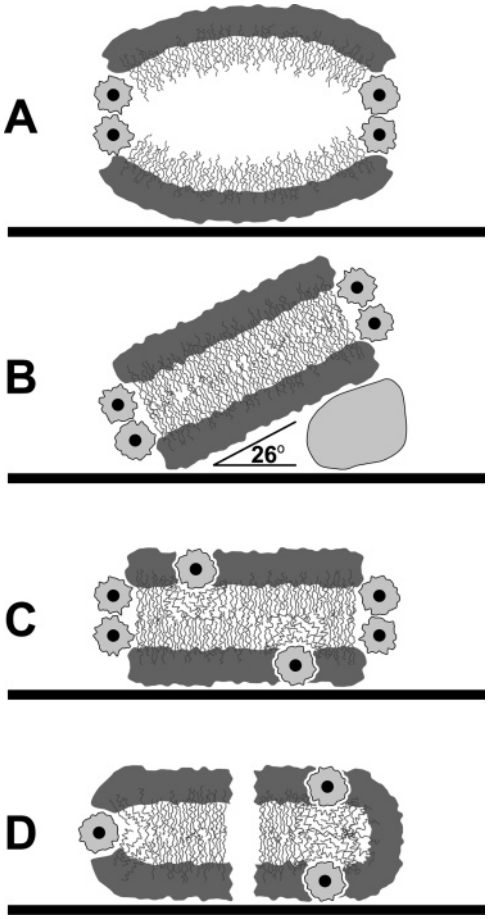

FIGURE 7: Models to account for reduced lipid acyl chain order relative to LpA-I, drawn to the same scale as in Figure 1 with the same schematic representation: (A) an ellipsoidal model, (B) bilayer model tilted at a 26° angle, (C) bilayer model with protein helices embedded in the interfacial region of the bilayer, and (D) alternative models for bilayer edge stabilization. A single helix is shown in the left panel, and micellar structure, perhaps stabilized by protein, in the right panel.

The particles examined were all approximately the same overall size, but this uniformity was a consequence of design rather than of nature. LpE-FL, LpE-TD_{10}, and even LpA-I, to some degree, may all be prepared with different lipid/protein ratios depending on the lipid and protein concentra-

tion of the suspension in which they are assembled, and this reflects the heterogeneity observed in vivo. For example, Koch et al. found that apoE-containing apoA-I-free lipoprotein particles in human cerebral spinal fluid were 18−22 nm in diameter (*55*), whereas LpE secreted by astrocytes of human apoE transgenic mice were only 12−14 nm in diameter (*56*). Although the studies described herein did not examine particles of different sizes and thus do not directly address how particle structures adjust to different ratios, our suggestion that lipids may stabilize at least portions of the bilayer disk perimeter in LpE-TD means that particle size is not determined by the amount of protein available for stabilizing the perimeter. LpE3-TD_{22} is an intriguing exception to this rule. Over a considerable range of lipid/protein ratios, LpE3-TD_{22} particles only form particles of the uniform size described above (S. Lund-Katz, M. C. Phillips, and K. H. Weisgraber, unpublished data).

Infrared spectra in the amide I region are quite sensitive to secondary structure, but there is no reliable procedure for translating spectra into quantitative or even qualitative assessments of such structure. The conundrum faced by those who would do so is made evident in tables provided by Goormaghtigh et al. (*57*) listing many spectral "assignments" that have been made in various proteins and peptides. Moreover, it is clear that different secondary structures have strikingly different absorption coefficients (*58*), as they should given that absorptivity is a sensitive function of dipolar coupling between peptide groups (*59*). The spectra reproduced in Figures 5 and 6 are consistent with mostly helical structure, but we believe that circular dichroism results reported in Table 1 provide better quantitative estimates of this structure. Thus, we subject our spectra to quantitative analysis not for estimates of secondary structure but to provide for a rational comparison of dichroic spectra and assessment of orientation (*39*, *41*). Nevertheless, the presence of a relatively well ordered component at 1629−1632 cm^{-1} in each of the particles that was examined (Tables 5 and 6) is strong evidence of secondary structure that is neither random nor helical. The high degree of orientational order in this component, its consistent presence in each of the particles, and various design features of the instrumentation (see Experimental Procedures) also weigh against the possibility that this component arises due to protein aggregation.

In conclusion, results indicate that there are no significant differences between the three isoforms of LpE-FL, and that different risk implications for the isoforms are not due to gross structural changes in LpE. The structural model that seems to best reconcile all the data is one in which full-length proteins largely assume an α-helical conformation, some of which is wrapped around a lipid bilayer disk (as in the belt model of LpA-I structure), and some of which is embedded horizontally in the bilayer.

ACKNOWLEDGMENT

We thank Dr. Karl Weisgraber and his colleagues Dr. Clare Peters-Libeu and Yvonne Newhouse for graciously providing LpE4-FL containing DPPC and DPPS, and David Nguyen for technical assistance.

SUPPORTING INFORMATION AVAILABLE

Ellipsoidal models of a distorted lipid bilayer yielding experimentally measured order parameters. This material is available free of charge via the Internet at http://pubs.acs.org.

REFERENCES

1. Mahley, R. W., and Rall, S. C., Jr. (2000) Apolipoprotein E: Far more than a lipid transport protein, *Annu. Rev. Genomics Hum. Genet. 1*, 507−537.
2. Roheim, P. S., Carey, M., Forte, T., and Vega, G. L. (1979) Apolipoproteins in human cerebrospinal fluid, *Proc. Natl. Acad. Sci. U.S.A. 76*, 4646−4649.
3. Pitas, R. E., Boyles, J. K., Lee, S. H., Hui, D., and Weisgraber, K. H. (1987) Lipoproteins and their receptors in the central nervous system. Characterization of the lipoproteins in cerebrospinal fluid and identification of apolipoprotein B,E(LDL) receptors in the brain, *J. Biol. Chem. 262*, 14352−14360.
4. Boyles, J. K., Zoellner, C. D., Anderson, L. J., Kosik, L. M., Pitas, R. E., Weisgraber, K. H., Hui, D. Y., Mahley, R. W., Gebicke-Haerter, P. J., and Ignatius, M. J. (1989) A role for apolipoprotein E, apolipoprotein A-I, and low density lipoprotein receptors in cholesterol transport during regeneration and remyelination of the rat sciatic nerve, *J. Clin. Invest. 83*, 1015−1031.
5. Corder, E. H., Saunders, A. M., Strittmatter, W. J., Schmechel, D. E., Gaskell, P. C., Small, G. W., Roses, A. D., Haines, J. L., and Pericak-Vance, M. A. (1993) Gene dose of apolipoprotein E type 4 allele and the risk of Alzheimer's disease in late onset families, *Science 261*, 921−923.
6. Saito, H., Lund-Katz, S., and Phillips, M. C. (2004) Contributions of domain structure and lipid interaction to the functionality of exchangeable human apolipoproteins, *Prog. Lipid Res. 43*, 350−380.
7. Weisgraber, K. H. (1994) Apolipoprotein E: Structure−function relationships, *Adv. Protein Chem. 45*, 249−302.
8. Westerlund, J. A., and Weisgraber, K. H. (1993) Discrete carboxyl-terminal segments of apolipoprotein E mediate lipoprotein association and protein oligomerization, *J. Biol. Chem. 268*, 15745−15750.
9. Wilson, C., Wardell, M. R., Weisgraber, K. H., Mahley, R. W., and Agard, D. A. (1991) Three-dimensional structure of the LDL receptor-binding domain of human apolipoprotein E, *Science 252*, 1817−1822.
10. Segelke, B. W., Forstner, M., Knapp, M., Trakhanov, S. D., Parkin, S., Newhouse, Y. M., Bellamy, H. D., Weisgraber, K. H., and Rupp, B. (2000) Conformational flexibility in the apolipoprotein E amino-terminal domain structure determined from three new crystal forms: Implications for lipid binding, *Protein Sci. 9*, 886−897.
11. Dong, J., Peters-Libeu, C. A., Weisgraber, K. H., Segelke, B. W., Rupp, B., Capila, I., Hernaiz, M. J., LeBrun, L. A., and Linhardt, R. J. (2001) Interaction of the N-terminal domain of apolipoprotein E4 with heparin, *Biochemistry 40*, 2826−2834.
12. Wilson, C., Mau, T., Weisgraber, K. H., Wardell, M. R., Mahley, R. W., and Agard, D. A. (1994) Salt bridge relay triggers defective LDL receptor binding by a mutant apolipoprotein, *Structure 2*, 713−718.
13. Fan, D., Korando, L. A., Dothager, R. S., Li, Q., and Wang, J. (2004) Complete ^{1}H, ^{13}C and ^{15}N assignments of a monomeric, biologically active apolipoprotein E carboxyl-terminal domain, *J. Biol. NMR 29*, 419−420.
14. Fan, D., Li, Q., Korando, L., Jerome, W. G., and Wang, J. (2004) A monomeric human apolipoprotein E carboxyl-terminal domain, *Biochemistry 43*, 5055−5064.
15. Fisher, C. A., and Ryan, R. O. (1999) Lipid binding-induced conformational changes in the N-terminal domain of human apolipoprotein E, *J. Lipid Res. 40*, 93−99.
16. Narayanaswami, V., Maiorano, J. N., Dhanasekaran, P., Ryan, R. O., Phillips, M. C., Lund-Katz, S., and Davidson, W. S. (2004) Helix orientation of the functional domains in apolipoprotein e in discoidal high-density lipoprotein particles, *J. Biol. Chem. 279*, 14273−14279.
17. Fisher, C. A., Narayanaswami, V., and Ryan, R. O. (2000) The lipid-associated conformation of the low-density lipoprotein receptor binding domain of human apolipoprotein E, *J. Biol. Chem. 275*, 33601−33606.
18. Narayanaswami, V., Szeto, S. S., and Ryan, R. O. (2001) Lipid association-induced N- and C-terminal domain reorganization in human apolipoprotein E3, *J. Biol. Chem. 276*, 37853−37860.
19. Drury, J., and Narayanaswami, V. (2005) Examination of lipid-bound conformation of apolipoprotein E4 by pyrene excimer fluorescence, *J. Biol. Chem. 280*, 14605−14610.
20. Lund-Katz, S., Zaiou, M., Wehrli, S., Dhanasekaran, P., Baldwin, F., Weisgraber, K. H., and Phillips, M. C. (2000) Effects of Lipid

Interaction on the Lysine Microenvironments in Apolipoprotein E, *J. Biol. Chem. 275*, 34459−34464.
21. Lund-Katz, S., Wehrli, S., Zaiou, M., Newhouse, Y., Weisgraber, K. H., and Phillips, M. C. (2001) Effects of polymorphism on the microenvironment of the LDL receptor-binding region of human apoE, *J. Lipid Res. 42*, 894−901.
22. Lund-Katz, S., Weisgraber, K. H., Mahley, R. W., and Phillips, M. C. (1993) Conformation of apolipoprotein E in lipoproteins, *J. Biol. Chem. 268*, 23008−23015.
23. Koppaka, V., Silvestro, L., Engler, J. A., Brouillette, C. G., and Axelsen, P. H. (1999) The Structure of Human Lipoprotein A-I: Evidence for the "Belt" Model, *J. Biol. Chem. 274*, 14541−14544.
24. Sparks, D. L., Lund-Katz, S., and Phillips, M. C. (1992) The charge and structural stability of apolipoprotein A-I in discoidal and spherical recombinant high-density lipoprotein particles, *J. Biol. Chem. 267*, 25839−25847.
25. Maiorano, J. N., and Davidson, W. S. (2000) The Orientation of Helix 4 in Apolipoprotein A-I-containing Reconstituted High-Density Lipoproteins, *J. Biol. Chem. 275*, 17374−17380.
26. Panagotopulos, S. E., Horace, E. M., Maiorano, J. N., and Davidson, W. S. (2001) Apolipoprotein A-I Adopts a Belt-like Orientation in Reconstituted High-Density Lipoproteins, *J. Biol. Chem. 276*, 42965−42970.
27. Morrow, J. A., Arnold, K. S., and Weisgraber, K. H. (1999) Functional characterization of apolipoprotein E isoforms overexpressed in *Escherichia coli*, *Protein Expression Purif. 16*, 224−230.
28. Saito, H., Dhanasekaran, P., Baldwin, F., Weisgraber, K. H., Lund-Katz, S., and Phillips, M. C. (2001) Lipid Binding-induced Conformational Change in Human Apolipoprotein E. Evidence For Two Lipid-Bound States On Spherical Particles, *J. Biol. Chem. 276*, 40949−40954.
29. Segall, M. L., Dhanasekaran, P., Baldwin, F., Anantharamaiah, G. M., Weisgraber, K. H., Phillips, M. C., and Lund-Katz, S. (2002) Influence of apoE domain structure and polymorphism on the kinetics of phospholipid vesicle solubilization, *J. Lipid Res. 43*, 1688−1700.
30. Liu, L., Bortnick, A. E., Nickel, M., Dhanasekaran, P., Subbaiah, P. V., Lund-Katz, S., Rothblat, G. H., and Phillips, M. C. (2003) Effects of apolipoprotein A-I on ATP-binding cassette transporter A1-mediated efflux of macrophage phospholipid and cholesterol: Formation of nascent high density lipoprotein particles, *J. Biol. Chem. 278*, 42976−42984.
31. Sparks, D. L., and Phillips, M. C. (1992) Quantitative measurement of lipoprotein surface charge by agarose gel electrophoresis, *J. Lipid Res. 33*, 123−140.
32. Lowry, O. H., Rosebrough, N. J., Farr, A. L., and Randall, R. J. (1951) Protein measurement with the Folin phenol reagent, *J. Biol. Chem. 193*, 265−275.
33. Bartlett, G. R. (1959) Phosphorus Assay in Column Chromatography, *J. Biol. Chem. 234*, 466−468.
34. Kucerka, N., Kiselev, M. A., and Balgavy, P. (2004) Determination of bilayer thickness and lipid surface area in unilamellar dimyristoylphosphatidylcholine vesicles from small-angle neutron scattering curves: A comparison of evaluation methods, *Eur. Biophys. J. 33*, 328−334.
35. Segrest, J. P., Jones, M. K., De Loof, H., Brouillette, C. G., Venkatachalapathi, Y. V., and Anantharamaiah, G. M. (1992) The amphipathic helix in the exchangeable apolipoproteins: A review of secondary structure and function, *J. Lipid Res. 33*, 141−166.
36. Tarek, M., Kechuan, T., Klein, M. L., and Tobias, D. J. (1999) Molecular Dynamics Simulations of Supported Phospholipid/Alkanethiol Bilayers on a Gold(111) Surface, *Biophys. J. 77*, 964−972.
37. Forte, T., and Nordhausen, R. W. (1986) Electron microscopy of negatively stained lipoproteins, *Methods Enzymol. 128*, 442−457.
38. Axelsen, P. H., Braddock, W. D., Brockman, H. L., Jones, C. M., Dluhy, R. A., Kaufman, B. K., and Puga, F. J., II (1995) Use of Internal Reflectance Infrared Spectroscopy for the in-situ Study of Supported Lipid Monolayers, *Appl. Spectrosc. 49*, 526−531.
39. Silvestro, L., and Axelsen, P. H. (1999) FTIR Linked Analysis of Conformational Changes in Annexin V Upon Membrane Binding, *Biochemistry 38*, 113−121.
40. Axelsen, P. H., Kaufman, B. K., McElhaney, R. N., and Lewis, R. N. A. H. (1995) The Infrared Dichroism of Transmembrane Helical Polypeptides, *Biophys. J. 69*, 2770−2781.
41. Axelsen, P. H., and Citra, M. J. (1996) Orientational order determination by internal reflection infrared spectroscopy, *Prog. Biophys. Mol. Biol. 66*, 227−253.
42. Koppaka, V., and Axelsen, P. H. (2001) Evanescent electric field amplitudes in thin lipid films for internal reflection infrared spectroscopy, *Langmuir 17*, 6309−6316.
43. Segrest, J. P., Jones, M. K., Klon, A. E., Sheldahl, C. J., Hellinger, M., De Loof, H., and Harvey, S. C. (1999) A Detailed Molecular Belt Model for Apolipoprotein A-I in Discoidal High-Density Lipoprotein, *J. Biol. Chem. 274*, 31755−31758.
44. Tam, S. P., and Breckenridge, W. C. (1983) Apolipoprotein and lipid distribution between vesicles and HDL-like particles formed during lipolysis of human very low-density lipoproteins by perfused rat heart, *J. Lipid Res. 24*, 1343−1357.
45. Innerarity, T. L., Pitas, R. E., and Mahley, R. W. (1979) Binding of arginine-rich (E) apoprotein after recombination with phospholipid vesicles to the low-density lipoprotein receptors of fibroblasts, *J. Biol. Chem. 254*, 4186−4190.
46. Marsh, D. (1990) *CRC Handbook of Lipid Bilayers*, CRC Press, Boca Raton, FL.
47. Acharya, P., Segall, M. L., Zaiou, M., Morrow, J., Weisgraber, K. H., Phillips, M. C., Lund-Katz, S., and Snow, J. (2002) Comparison of the stabilities and unfolding pathways of human apolipoprotein E isoforms by differential scanning calorimetry and circular dichroism, *Biochim. Biophys. Acta 1584*, 9−19.
48. Koppaka, V., and Axelsen, P. H. (1999) Lipoprotein A-I structure, *Trends Cardiovasc. Med. 9*, 192−195.
49. Li, H. H., Lyles, D. S., Thomas, M. J., Pan, W., and Sorci-Thomas, M. G. (2000) Structural determination of lipid-bound ApoA-I using fluorescence resonance energy transfer, *J. Biol. Chem. 275*, 37048−37054.
50. Tricerri, M. A., Agree, A. K. B., Sanchez, S. A., Bronski, J., and Jonas, A. (2001) Arrangement of apolipoprotein A-I in reconstituted high-density lipoprotein disks: An alternative model based on fluorescence resonance energy transfer experiments, *Biochemistry 40*, 5065−5074.
51. Klon, A. E., Segrest, J. P., and Harvey, S. C. (2002) Comparative models for human apolipoprotein A-I bound to lipid in discoidal high-density lipoprotein particles, *Biochemistry 41*, 10895−10905.
52. Li, L., Chen, J. G., Mishra, V. K., Kurtz, J. A., Cao, D. F., Klon, A. E., Harvey, S. C., Anantharamaiah, G. M., and Segrest, J. P. (2004) Double belt structure of discoidal high-density lipoproteins: Molecular basis for size heterogeneity, *J. Mol. Biol. 343*, 1293−1311.
53. Raussens, V., Fisher, C. A., Goormaghtigh, E., Ryan, R. O., and Ruysschaert, J. M. (1998) The low-density lipoprotein receptor active conformation of apolipoprotein E: Helix organization in N-terminal domain-phospholipid disc particles, *J. Biol. Chem. 273*, 25825−25830.
54. Lund-Katz, S., Anantharamaiah, G. M., Venkatachalapathi, Y. V., Segrest, J. P., and Phillips, M. C. (1990) Nuclear magnetic resonance investigation of the interactions with phospholipid of an amphipathic α-helix-forming peptide of the apolipoprotein class, *J. Biol. Chem. 265*, 12217−12223.
55. Koch, S., Donarski, N., Goetze, K., Kreckel, M., Stuerenburg, H. J., Buhmann, C., and Beisiegel, U. (2001) Characterization of four lipoprotein classes in human cerebrospinal fluid, *J. Lipid Res. 42*, 1143−1151.
56. Fagan, A. M., Holtzman, D. M., Munson, G., Mathur, T., Schneider, D., Chang, L. K., Getz, G. S., Reardon, C. A., Lukens, J., Shah, J. A., and LaDu, M. J. (1999) Unique lipoproteins secreted by primary astrocytes from wild type, apoE (−/−), and human apoE transgenic mice, *J. Biol. Chem. 274*, 30001−30007.
57. Goormaghtigh, E., Cabiaux, V., and Ruysschaert, J. M. (1994) Determination of Soluble and Membrane Protein Structure by Fourier-Transform Infrared Spectroscopy. III. Secondary Structures, *Subcell. Biochem. 23*, 405−450.
58. de Jongh, H. H., Goormaghtigh, E., and Ruysschaert, J. M. (1996) The different molar absorptivities of the secondary structure types in the amide I region: An attenuated total reflection infrared study on globular proteins, *Anal. Biochem. 242*, 95−103.
59. Paul, C., Wang, J. P., Wimley, W. C., Hochstrasser, R. M., and Axelsen, P. H. (2004) Vibrational coupling, isotopic editing, and β-sheet structure in a membrane-bound polypeptide, *J. Am. Chem. Soc. 126*, 5843−5850.

BI050872J